Laser-Induced Graphene Formation on Recycled Woods for Green Smart Furniture

*Han Ku Nam, Jungrak Choi, Tongmei Jing, Dongwook Yang, Younggeun Lee, Young-Ryeul Kim, Truong-Son Dinh Le, Byunggi Kim, Liandong Yu, Seung-Woo Kim, Inkyu Park, and Young-Jin Kim**

Dr. H. K. Nam, Dr. J. Choi, T. Jing, D. Yang, Y. Lee, Y.-R. Kim, Prof. S.-W. Kim, Prof. I. Park, Prof. Y.-J. Kim
Department of Mechanical Engineering, Korea Advanced Institute of Science and Technology (KAIST), Science Town, Daejeon, 34141, South Korea

E-mail: yj.kim@kaist.ac.kr

T. Jing, Prof. L. Yu
Department of Control Science and Engineering, China University of Petroleum (East China), Qingdao, 266580, China

Dr. T.-S. D. Le
Department of Biomedical Engineering, National University of Singapore, Singapore, 117583, Singapore

Dr. B. Kim
Institute of Industrial Science, The University of Tokyo, Tokyo, 153–8505, Japan

Keywords: smart furniture, green, laser-induced-graphene, recycled wood, direct laser writing

In the pursuit of carbon neutrality policies, the development of eco-friendly and intelligent furniture commands a significant role. However, the integration of non-biodegradable electronic components in smart furniture fabrication has led to substantial electronic waste. Here, we report a straightforward approach, the rapid production of Laser-Induced Graphene (LIG) on medium-density fiberboard (MDF), a prevalent recycled wood in furniture production. This LIG electrode is crafted with negligible material ablation in ambient air with the aid of femtosecond laser pulses, without requiring any additional materials, showcasing the highest electrical conductivity (2.781 Ω sq^{-1}) among previously reported lignocellulosic materials-

based LIG. The application of this LIG electrode for lighting, heating, and touch sensors displays sufficient performance for smart furniture implementation. For eco-conscious furniture, LIG-based human-machine interfaces are demonstrated on recycled woods for the facile control of smart devices, which will readily enable IoT-oriented smart sustainable furniture.

1. Introduction

As industrialization forges ahead, the pressing issue of accelerated global warming and intensifying climate change comes to the fore.[1] A pivotal driver behind this transformation is the escalation of greenhouse gas emissions, with the foremost contributor being CO_2. These emissions have surged, elevating the global atmospheric concentration by 46% from 1850's 285 ppm to 2020's 415 ppm, thereby elevating the average global surface temperature by ~1.2 ℃.[2] In response to this environmental imperative, nations are engaging in carbon neutrality policies, echoed by scholars underscoring the imperative of research and development to curtail greenhouse gas emissions.[3,4] A standout strategy in the pursuit of carbon neutrality is the adoption of wood-based materials, renowned for their eco-friendliness. While wood offers virtues of renewability, abundance, biodegradability, cost-efficiency, carbon neutrality, and pollution reduction, the predicament of managing discarded wood remains partially unresolved.[5] Rigorous efforts are directed at recycling wood waste to mitigate this challenge, aligning with European Union (EU) targets to achieve a 20% wood recycling rate by 2025 and 30% by 2030. Notably, recycled wood predominantly finds application in thermal power generation or as a basis for reconstituted wood products like Particleboard (PB) and medium-density fiberboard (MDF).[6] Furthermore, to enhance the utilization of wood, ongoing efforts are directed toward the development of various technologies encompassing mechanical, chemical, and thermal modifications for overcoming the limitations of wood.[7] These include the advancement of wood-plastic composite manufacturing technology, aimed at cost-effectiveness and superior performance compared to conventional wood materials, densified wood manufacturing technology was invented to enhance mechanical properties through chemical treatment and compression.[8,9] These also include wood-based antibacterial structural material production technology, achieved through chemical treatment and heat pressure treatment, as well as 3D molded wood production technology, which manipulates the wood cell wall structure.[10,11] Moreover, transparent wood production technology, achieved through delignification and polymer infiltration, represents another avenue of ongoing research.[12] Collectively, these diverse technological advancements signify a continuous pursuit towards optimizing the utilization of wood resources. Produced engineered wood holds significant promise for enhanced applications in the wooden furniture and construction sectors, owing to its markedly improved performance.[13] For instance, densified wood with enhanced strength can serve as a robust building frame, transparent wood can be utilized as a substitute for traditional glass windows, and delignified white wood can offer an efficient cooling solution when used as a roofing material.[14–16] These advancements underscore the potential of engineered wood to

revolutionize various industries, offering sustainable and innovative solutions for modern construction/furniture and design challenges.

As the global movement towards eco-friendliness gains momentum, there's a rising demand for wooden furniture that aligns with low greenhouse gas emissions.[17] Wood-based furniture, with its durability, minimal upkeep, health advantages, and robust structural integrity, contributes to a steady 4.4% annual growth in the wood furniture market while also addressing recycling concerns and boasting biodegradability and sustainability as a green material.[18] In contrast to plastics and metals, often used in furniture, wood stands out due to its inherent recyclability, readily transformed into MDF and PB plates for furniture production. However, this recycled wooden furniture often lacks conductivity, posing challenges in an era where households increasingly seek smart solutions. There is currently no precise definition for the implementation of smart furniture until now.[19] However, various researchers argue that smart furniture should possess the capability to communicate with users and anticipate their needs through an array of sensors and actuators integrated into the user's environment.[20] Essentially, this smart furniture should cater specifically to the requirements of its users. To bring such smart furniture to life, a necessary component is the human-machine interface (HMI). HMI serves to enhance and simplify the interaction between a computer or other mechanical devices and the user, enabling the user to oversee and control the machinery or system. In simpler terms, the realization of smart furniture relies on the development of a system integrated into the furniture, capable of receiving, processing, and executing user requirements. Thus, the inconvenience of incorporating separate electronic devices for various functions has emerged. This predicament can be circumvented by imbuing furniture with inherent conductivity. Various methods have emerged for rendering wood-based materials to be electrically conductive, including metal-coating/post-melting, copper wire coating, sputtering-based coating, and blending the wood powder with polyvinyl to craft conductive hydrogels.[21–24] Notably, these approaches necessitate additive integration of other materials through coating, doping or blending, which could set drawbacks in terms of production time, volume, and biodegradability or biocompatibility of the added materials.[25] In the pursuit of green electronics, several criteria must be met.[26] Firstly, precursors should be abundant, cost-effective, and organic in nature. Additionally, the synthetic routes employed should be economically feasible, with high production rates, and the fabrication processes for synthesized electronic materials should be low-cost. Moreover, for a device to be truly green, it should be biodegradable and biocompatible. In summary, utilizing lignocellulosic materials as precursors, which can be

economically manufactured with high production rates, while meeting criteria such as biodegradability and biocompatibility, holds the promise of creating an ideal smart green furniture solution.

In 2017, Prof. Tour's group showcased the successful creation of Laser-Induced Graphene (LIG) through continuous-wave (CW) laser irradiation on wood, establishing the feasibility of crafting carbon electrodes directly onto wood-based materials without addition of other conductive materials.[27] LIG emerges via laser irradiation on carbon precursors, inducing photochemical and photothermal transitions that lead to the exclusive retention and reconfiguration of carbon constituents.[28] This process engenders a three-dimensional (3D) porous structure, evolving from the gas release generated during the material's laser-induced decomposition.[29] Notably, LIG's swift and facile electrode production, in contrast to earlier graphene fabrication methods, has attracted considerable attention, fueling an ongoing exploration of its application to diverse wood-based substrates. Given wood's susceptibility to combustion, various strategies such as defocusing and multi-lasing techniques,[29] or generating LIG within a nitrogen environment to quell oxygen-induced combustion.[30] For higher productivity and higher precursor-to-LIG conversion ratio in ambient air, the ultrashort femtosecond pulse lasers have been introduced, so as to create LIG on trees and leaves in non-thermal manner with minimal ablation.[31,32] Due to their ultra-short pulse duration in the time domain, femtosecond lasers excel at minimizing heat diffusion, leading to a substantial enhancement in the spatial resolution of graphene electrodes. Furthermore, the high repetition rate of pulses can facilitate precise heat accumulation and efficiently transform carbon precursors into high-quality graphene with exceptional electrical conductivity. Subsequently, research has expanded to demonstrate LIG synthesis on lignocellulosic materials like paper, cellulose paper, cork, and potato peel.[33–35] These advancements have facilitated applications in micro-supercapacitors, temperature and chemical sensors, biosensors, and food monitoring. However, despite the increasing interest and demands in wood recycling and smart furniture recycling, there has been no research on generating LIG from recycled wood materials, such as MDF and Particle Board, nor have there been any reported attempts to incorporate LIG electrodes into furniture for green smart furniture.

In this study, we harnessed femtosecond laser direct writing (FsLDW) technology to craft high-quality LIG onto recycled wood, subsequently integrating it into the realm of green smart furniture fabrication. Through the precise deployment of femtosecond laser pulses with a high

repetition rate, low absorption of near-infrared (NIR) wavelength, and an ultrashort pulse duration, localized thermal energy was delivered to the target area. This strategy not only prevented ablation in the ambient air environment but also instigated photothermal-induced graphitization within the recycled wood. High-quality LIG electrodes, achieving an impressive electrical conductivity of 2.781 $\Omega\ sq^{-1}$, were successfully crafted on MDF with minimal ablation depth (25 μm) under optimized conditions. Recognizing MDF's widespread use as an eco-friendly furniture material, we developed technology to elevate furniture into the realm of smart design, seamlessly integrating LIG-based touch sensors, electric wire for lighting, and heaters into environmentally conscious smart green furniture. Leveraging MDF's popularity and sustainability credentials, we broadened the horizons of LIG electrode applications. Our FsLDW technology-derived LIG electrodes effortlessly accommodate the incorporation of touch sensors, heaters, and lighting in customizable configurations, circumventing the need for supplementary processing or intricate installation procedures. This amalgamation of attributes concurrently paves the way for mass production and tailored manufacturing, a symbiotic fusion that addresses diverse individual preferences. Moreover, smart furniture manufactured in this manner can be implemented economically and rapidly, possesses biodegradability and biocompatibility, and aligns with the principles of green electronics. MDF serves both as a substrate and a carbon electrode precursor without additional chemicals, meeting the criteria for perfect green electronics. Furthermore, this technology inherently resolves the recycling quandary associated with smart furniture, mitigating the electronic waste predicament and increasing the hallmark quality and cost-effectiveness of MDF furniture. This technology thus presents a significant stride in the domain of IoT-driven, sustainable, and intelligent furniture solutions.

2. Results and Discussion

[One-step Fabrication of FsLDW-based LIG electrodes on Recycled Wood]

In this study, recycled wood was employed as a cost-effective and eco-friendly precursor for the development of smart furniture technologies, including touch sensors, electric wires for lighting, and stove warmers, achieved through large-scale production of high-quality graphene, as shown in Figure 1. High-quality LIG electrodes, swiftly produced on recycled wood using the FsLDW, can readily be employed in various smart furniture applications without requiring additional treatment. This potential highlights the capacity for adding substantial value to recycled wood products. Recycled wooden materials, namely Medium Density Fiberboard (MDF), Particle Board (PB), Oriented Strand Board (OSB), and Lumber Core Plywood (LCP), are used here for the production of LIG. MDF, PB, and OSB share a common production process involving crushed wood pieces combined with adhesives and subjected to thermal compression, but the particle size is different. However, LCP diverges from this by utilizing plywood as a core with veneers attached to its exterior. Efforts to carbonize and graphitize lignocellulosic materials, including wood, have been long-standing. During pyrolysis under oxygen-suppressed conditions, the original cell wall structure of wood and biomass sources is disrupted.[36] Nanocrystalline graphite grows at temperatures between 600-900 ℃, and two-dimensional graphene is partially formed at 1000 ℃.[37] In aromatic compounds such as lignin fulfill an important function, undergoing dehydrogenation/graphitization reactions at higher activation temperatures, producing poly-nuclear aromatic hydrocarbons, and enhancing carbonization.[38] Cellulose, devoid of aromatic carbon, transforms into aromatic carbon, with temperature-dependent processes involving desorption of physically adsorbed water below 150 ℃, dehydration between 150-240 ℃, depolymerization and bond breakage between 240-400 ℃, and formation of an aromatization or graphite-like layer beyond 400 ℃.[39,40] At lower pyrolysis temperatures, cellulose converts into a carbonaceous material with high oxidation degrees, transitioning to sp^2 carbon-rich structures with increased graphitization as temperatures rise.[41] Moreover, a catalyst-based approach has been developed to induce graphitization of lignocellulosic materials at relatively lower temperatures.[42] Metal catalysts like iron and nickel facilitate graphite production by lowering the graphitization conversion temperature. Additionally, a method has been introduced to convert amorphous carbon in wood char into carbon nanotubes (CNTs) solely through joule heating, without additional materials.[43] Amorphous carbon's nonuniform structure results in resistance variation at different positions, whereby joule heating up to 3000 K, with oxygen suppressed, elevates the temperature at high-

resistance sites, prompting carbon sublimation. The sublimated carbon, trapped in a one-dimensional container, reassembles into crystalline CNTs. Nevertheless, the graphitization process of diverse lignocellulosic materials faces limitations concerning time, cost, and design flexibility for green electronics fabrication. To address these constraints, we sought to form a carbon electrode by inducing an appropriate photothermal effect using femtosecond laser pulses. Through exposure to a femtosecond pulse laser in an ambient atmosphere, high-quality LIG was generated. The unique advantage of femtosecond lasers lies in their ability to facilitate high-resolution processing via non-thermal ablation or nonlinear optical mechanisms such as multi-photon absorption.[44] This approach ensures the swift and efficient fabrication of superior graphene electrodes in ambient air, while mitigating undesired thermal effects.[45] Remarkably, the low absorption rate of near-infrared wavelengths on wood, typically below 20%, is surmounted by the femtosecond laser's capacity for multi-photon absorption, enabling direct LIG electrode creation on wood surfaces.[46] Leveraging its relatively low absorption of NIR wavelengths, the femtosecond laser minimizes ablation depth compared to UV and visible light sources. This property assists in the penetration of thermal energy, yielding thicker LIG electrodes. The optimization of production speed was achieved by a strategy involving rapid interior filling following a slower rim drawing process. Employing a high repetition rate of 200 kHz pulse trains facilitated efficient heat accumulation, thus accelerating LIG conversion through photothermal effects. Patterning on recycled woods (MDF, PB, OSB, LCP) encompassed a range of laser scan speeds (10 to 50 mm/s) and laser powers (0.8 to 1.5 W) to identify the ideal conditions for achieving optimal LIG electrical conductivity (Figure S1, Table S1-4). Notably, PB, OSB, and MDF exhibited wide-ranging capabilities for producing LIG electrodes. In contrast, LCP, comprised of veneer softwood, faced challenges in generating high-quality electrodes due to increased susceptibility to ablation. OSB's larger wood pieces led to local voids, preventing uniform LIG electrode formation. MDF, with its smaller wood fragments, consistently yielded the most uniform LIG results, boasting lower sheet resistance values attributed to its inherent structural stability. Consequently, MDF underwent further parametric testing at conditions spanning 10 to 90 mm/s and 0.8 to 3 W, yielding a LIG electrode with remarkable electrical conductivity of 2.78 Ω sq^{-1} under 2W and 30 mm/s conditions. In contrast, PB exhibited relatively higher sheet resistance, particularly at lower speeds. OSB, due to its larger wood particles, demonstrated instability in LIG formation, likely stemming from reduced thermal conductivity impeding heat dissipation during laser pulses, yielding non-uniform LIG.[47] Notably, the optimized MDF-derived LIG exhibited outstanding electrical conductivity even without additional fire-retardant treatment, surpassing the

performance of various lignocellulose-based LIG electrodes outlined in Table 1. Specifically, the sheet resistance of the femtosecond laser-produced MDF LIG was the best result, reflecting a remarkable 2.61-fold enhancement in conductivity compared to prior studies' best conditions. This achievement can be attributed to MDF's structurally robust composition resulting from heat and compression during manufacturing, facilitating efficient conversion into a graphene structure while minimizing undesirable ablation during LIG formation.

Figure 1. Illustration, modelling sample, and concept image of LIG touch sensor, electric wire for lighting, and stove warmer for green smart furniture applications.

Table 1. Comparison of lignocellulosic materials based LIG.

Materials	Sheet Resistance (Ω sq^{-1})	Chemical / Metal Doping	I_D/I_G	Laser Type	Application	Ref, (Year)
Wood (Pine, Birch, Oak)	10	×	0.85, 0.73, 0.48	CO_2 laser under Ar or H_2	❶Electrodes, ❷Supercapacitors	[27] (2017)
Wood (Cedar)	7	NiFe (Soaked in chemical solution)	0.3 to 0.6	CO_2 laser under Ar	❶Electrode, ❷Electro-magnetic interference shielding material	[48] (2018)
Wood	20	Iron (Iron-tannic acid ink)	-	CO_2 laser	❶Strain sensors, ❷Flexible electrodes, ❸Capacitive touch panels	[49] (2022)
Wood (Bamboo)	-	×	0.7	Femtosecond laser	Supercapacitors	[50] (2022)
Wood (Mulbau, Rubber, Acacia, Walnut, Bamboo)	6	×	0.25	Femtosecond laser	❶Temperature sensor, ❷Heater, ❸Boiler, ❹Electrical interconnections	19 (2023)
Wood (Softwoods and Hardwoods)	10	MnO_2	0.63	Femtosecond laser	❶Sensors, ❷Pseudo-capacitors	[45] (2019)
Leaves						
Leaves	23	×	≈ 0.8	Femtosecond laser	Micro-supercapacitors	18 (2022)
Coconut surface	8	×	0.6	CO_2 laser	Micro-supercapacitor	[29] (2018)
Potato surface						
Filter paper						
Wood						
Paper cup	105	×	≈ 0.8	Nd:YAG continuous-wave laser	Food monitoring sensor	[34] (2022)
Filter paper	32	×	0.5	CO_2 laser	Strain sensor	[51] (2021)
Cotton fiber watercolor paper	40	×	1.0	CO_2 laser	Art production	[52] (2019)
Cork	115	×	≈ 0.6	CO_2 laser	Triboelectric nanogenerators	[53] (2019)
Cork (Cork oak trees)	LIG: 46 Boron LIG：38	Boron-doped (H_3BO_3)	1.0	Diode laser	Micro-supercapacitor	[35] (2022)
Cork （Natural cork and Agglomerate cork）	75	×	0.41	Diode-pumped Nd:YVO_4 pulsed laser	Piezoresistive sensors	[54] (2020)
Cork (Amorim cork)	10	×	0.2	CO_2 laser, NIR fiber laser	Micro-supercapacitors	[55] (2022)
Lignin (Softwood, Kraft lignin)	306	×	≈ 0.6	Femtosecond laser	Flexible supercapacitors	[56] (2021)
Lignin (Softwood, Kraft lignin)	-	×	≈ 2.2	CO_2 laser	Flexible supercapacitors	[57] (2020)
Lignin (Alkali lignin)	-	×	-	Femtosecond laser	Triboelectric nanogenerators	[58] (2023)
MDF	2.781	×	0.57	Femtosecond laser	❶Heater, ❷Touch sensor ❸Electric wire for lighting	This work 2023

'-': Undisclosed
'≈': Approximate expected value based on provided graph
'×': Undoped

[Characterization of LIG Electrodes on MDF]

Figure 2a and 2b illustrate the SEM images of MDF and LIG, offering results in their distinctive characteristics. For MDF, the image reveals the presence of intricately interwoven wood particles spanning tens to hundreds of micrometers. This composite is achieved through a rigorous amalgamation of wood fiber fragments with thermosetting Resin, such as urea, phenol, or melamine-formaldehyde, followed by high-temperature and high-pressure treatment during MDF fabrication.[59] Contrarily, the optimal condition of 2 W and 30 mm/s displays a porous structure under high magnification (2,000 X), accompanied by stuck formations at lower magnifications (200 X). This phenomenon stems from the resin used in MDF production, wherein some remnants affect the manufacturing process result. This attribute, advantageous for sustaining mechanical stability, fosters a porous electrode suited to diverse applications. The porous structure is also evident in biochar generated through pyrolysis. At temperatures exceeding 900°C, the wood undergoes carbonization and graphitization processes, with lateral growth of graphene sheets persisting.[60] Concurrently, closed micropores begin to form as atomic ordering reduces the interlayer spacing. Additionally, as depicted in Figure S2, SEM examinations undertaken across speeds of 10 to 80 mm/s, under the 2 W power setting of the near-infrared femtosecond laser, elucidate the microstructure of the electrode. This approach unveils the porous framework ensuing from the swift release of gas molecules (CO, H_2, etc.) generated via organic material decomposition and rearrangement, alongside the transformation and regeneration of the extant microstructure into graphene. The ultrashort laser irradiation initiates the rupture of covalent bonds within MDF's internal components (lignin, hemicellulose, cellulose) via photon energy, prompting ablation and swift temperature escalation.[61] These conditions induce the momentary formation of remarkably high pressures.[62] From a material conversion standpoint using laser photon energy, ultrashort laser pulses can induce a transition from amorphous to crystalline states. This transition occurs through the excitation of a dense electron-hole plasma, leading to an ultrafast non-thermal phase change that outpaces thermally activated transitions.[63] Covalent materials like carbon experience such ultrafast nonthermal phase shifts under irradiation by femtosecond laser pulses.[64] These pulses generate a dense electron-hole plasma that alters the potential energy surface, prompting the transition from amorphous to crystalline states. Given that sp^2-hybridized orbitals are generally more stable than sp^3, the rearrangement of atoms in amorphous carbon tends to favor the formation of graphitic layers.[65] This inclination towards graphitization is particularly pronounced under high temperature and pressure conditions. Within such high-temperature, high-pressure confines, residual carbons coalesce, yielding graphene endowed with a three-dimensional porous

structure.[64] Notably, conditions of severe ablation (10, 20 mm/s) yield substantial chunks, while relatively optimal settings of 30 to 60 mm/s foster an apt porous structure. Localized LIG formations with numerous defects or voids transpire at elevated speeds (70 to 80 mm/s). This compilation of findings affirms that distinct laser power outputs significantly modulate processing dynamics. In Figure S3, outcomes from confocal microscopy analysis discern differences between LIG and MDF generated using a laser output of 2 W and 30 mm/s, quantified as a 25.02 μm depth variance, symbolizing the ablation depth attributed to laser-induced photothermal effects. In contrast, a 2 W, 7 mm/s configuration amplifies the difference to 114.4 μm between MDF and the outline, intensifying ablation depth due to heightened energy, albeit at the expense of LIG performance. The findings show that high electrical conductivity LIG electrodes can be formed, achieved through a judicious allocation of energy at optimal laser power and scan speed, effectively mitigating ablation depth. Figure S4 shows average roughness measurements through confocal microscopy, indicating a R_a of 7.698 μm for MDF and 16.83 μm for LIG, spotlighting escalated surface roughness attributed to porous graphene structure generation via laser irradiation.

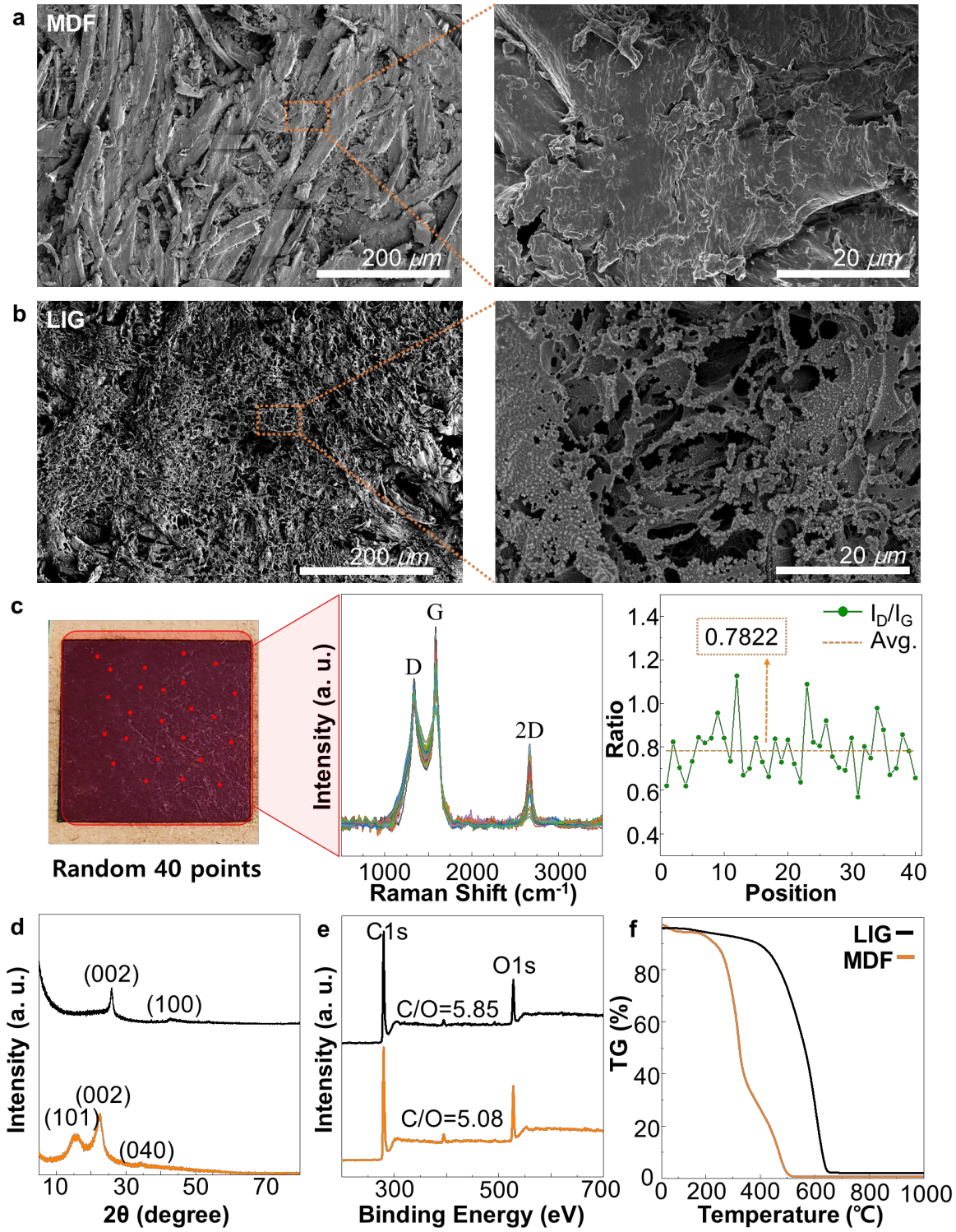

Figure 2. LIG and MDF analysis. **(a)** SEM images of MDF. **(b)** SEM images of LIG on MDF. **(c)** Raman spectrum results of LIG on MDF with random 40 points. **(d)** XRD spectra, **(e)** XPS spectra, and **(f)** TGA spectra of MDF and LIG on MDF.

Figure 2c shows the 40 random points of Raman spectra, unveiling essential features of the examined LIG samples. The D band, centered at 1345 cm^{-1}, signifies an intrinsic phonon mode of aromatic rings with A_{1g} symmetry, indicating the presence of defects within the

disordered graphene. Conversely, the G band, positioned at 1587 cm^{-1}, corresponds to the hexagonal carbon structure, reflective of sp^2 hybridized carbon atoms' E_{2g} vibrational mode. The appearance of the 2D band at 2670 cm^{-1}, the secondary signal of the D band, denotes the production of multi-layered graphene. The best result of generated LIG electrode demonstrates promise with an I_D/I_G ratio of 0.57, which represents a low value indicating high quality. Considering the inherent heterogeneity of the wood material, which serves as a carbon precursor, as well as the irregular porous structure of LIG formed due to gas emission during laser pulse-induced decomposition, Raman analysis was conducted on 40 random points. With an average I_D/I_G value of 0.7822, the majority of LIGs exhibited excellent quality, with only two points exceeding a value of 1. The incident ultrashort laser pulse elevates the temperature of the electron gas to exceedingly high levels, placing it in a non-equilibrium state.[62] Initially, the force field within graphite undergoes modification due to electronic excitations, which diminish interlayer interactions, and notably, through Coulomb interaction among the charged graphene monolayers. This Coulomb repulsion force leads to the exfoliation of the upper graphene layer. However, given that the pulse duration exceeds several tens of femtoseconds, the likelihood of exfoliating multilayer graphene rather than a single layer increase. As seen in Figure 2d, 2e, and 2f, X-ray Diffraction (XRD), X-Ray Photoelectron Spectroscopy (XPS), and Thermogravimetric Analysis (TGA) analyses were conducted on LIG and MDF. The crystalline structure of LIG in MDF was examined using XRD analysis, which revealed a spectrum of MDF displaying three distinct peaks: (101), (002), and (040). These peaks undergo shifts, attenuation, or disappearance as MDF is transformed by LIG. These findings suggest alterations in the structure of MDF following femtosecond laser irradiation. In LIG's XRD spectrum, a conspicuous (002) peak is observed around $2\theta = 25.9°$, indicating the successful formation of aromatic graphene with an interlayer spacing of 0.34 nm. LIG's double-layer graphene-like structure emerges at appropriately elevated temperatures (2,400 to 3,000 K), exhibiting interlayer spacing akin to graphite structure.[61] Nonetheless, the interlayer spacing between two adjacent lattice surfaces in the outer region of the generated LIG may exhibit slight variations due to the presence of pentagonal or heptagonal aromatic rings, in contrast to the typical hexagonal structure.[66] Pentagonal and heptagonal carbon structures are typically found at the edges rather than within the carbon plane. Moreover, the predominance of forming hexagonal structures over pentagonal and heptagonal structures at a temperature of 3000 K compared to 2400 K suggests that the growth of pentagonal and heptagonal structures might be more energetically favorable in the absence of a metal catalyst. Furthermore, higher temperatures increase the proportion of 2D-connected hexagonal rings, thereby enhancing crystallinity.[67]

They coexist with most non-carbon atoms, such as oxygen and nitrogen, and these non-carbon atoms can serve as intermediaries in the formation of carbon rings. The removal of non-carbon atoms involves overcoming specific energy barriers, implying that higher temperatures or increased energy levels may be necessary. In simpler terms, this process entails opening and subsequently recombining the existing hexagonal carbon rings, with a minimum estimated temperature of approximately 2,100 K. Nevertheless, suitably elevated temperatures facilitate the formation of LIG with an interlayer spacing akin to that of single- or double-layer graphene. In contrast to theoretical approaches based on molecular dynamics simulation, our experimental setup involves directly irradiating femtosecond laser pulses onto wood in ambient air. Consequently, minimizing ablation of the wood substrate becomes a simultaneous concern. This highlights the necessity of manufacturing LIG electrodes under optimal conditions to ensure both high conductivity and the prevention of substrate damage. XPS analysis was employed to further assess the chemical structure and material composition of both MDF and LIG surfaces. The C/O atomic ratio for MDF was determined to be 5.08, while LIG exhibited a higher ratio of 5.85. This result suggests that some oxygen-containing functional groups were eliminated during the graphene formation process, confirming the successful creation of a graphene structure. The elevated proportion of non-carbon atoms in comparison to single-layer and few-layer graphene can be inferred through the exposition of the LIG formation mechanism elucidated earlier. Within this intricate process, non-carbon atoms, namely oxygen and nitrogen, assume the pivotal role of facilitating carbon-ring formation in the outermost periphery. This phenomenon expedites the rapid formation of LIG, albeit at the expense of a slightly higher oxygen ratio. However, the limited presence of hydrogen can be attributed to the predominant generation of carbon monoxide (CO) during the decomposition phase of the initial material in LIG production, whereas hydrogen gas (H_2) is primarily emitted during the subsequent reassembly phase.[66] Lastly, TGA systematically assessed the thermal stability of both LIG and MDF. In the case of MDF, the analysis revealed the evaporation of internal moisture at temperatures of 100 ℃ or higher, followed by the onset of decomposition around 200 ℃. Subsequently, a rapid mass loss occurred in the temperature range of 240 to 340 ℃, attributed to the decomposition of cellulose and hemicellulose. The decomposition rate exhibited a reduction in the 340 to 500 ℃ range due to the enhanced thermal stability of the aromatic carbon rings present in lignin. The final stages of decomposition, including the residual compounds like ash, occurred around 500 ℃. On the other hand, LIG displayed a decomposition range of 430 to 650 ℃, suggesting relatively higher thermal stability compared to MDF.

[Demonstration of LIG-based Smart Touch Sensor on MDF]

The initiation of smart furniture can be considered to commence with the utilization of the touch sensor. This pivotal component serves as the foundation for the operation of a wide spectrum of electronic devices, encompassing appliances such as refrigerators, televisions, heaters, and computers. Leveraging the prevalent use of MDF in wooden furniture, capacitive LIG touch sensors were directly fashioned using the FsLDW technology, as depicted in Figure 3. To safeguard the LIG electrode, the fabricated touch sensor was coated with wooden varnish. Figure 3a exhibits the on/off control functionality of the LIG touch sensor, characterized by its rapid response time of 1/1200 of a second. Significantly, a range of touch methods including quick taps, slow taps, presses, double taps, multitaps, and long presses, yielded fast responses. This LIG touch sensor extended to LED brightness modulation, exemplified in Figure 3b. Employing a PWM (Pulse Width Modulation) methodology, the LED bulb's luminosity was adeptly governed, enabling incremental adjustments from 30% to 90% and culminating in a complete shutdown at the fourth touch. Furthermore, a precautionary measure was implemented to activate power upon the hand's descent, rather than upon initial contact, to mitigate inadvertent activations. Figure 3c underscored the concurrent control of multiple touch sensors, gauging their organic responsiveness in alignment with prevalent touch panel capabilities. Furthermore, considering wrong capacitive measures, a threshold was established to effectively minimize the likelihood of malfunctions when a hand approaches the sensor's periphery. In pursuit of tangible applicability to smart furniture, seven touch sensors were crafted and endowed with specific functions, including continuous movement scenarios (e.g., T1 → T3), solidifying the potential for MDF-based green smart LIG sensors to supplant essential touch sensor roles in the realm of smart homes and furniture by controlling computer as seen in Figure S5, and Video S1.

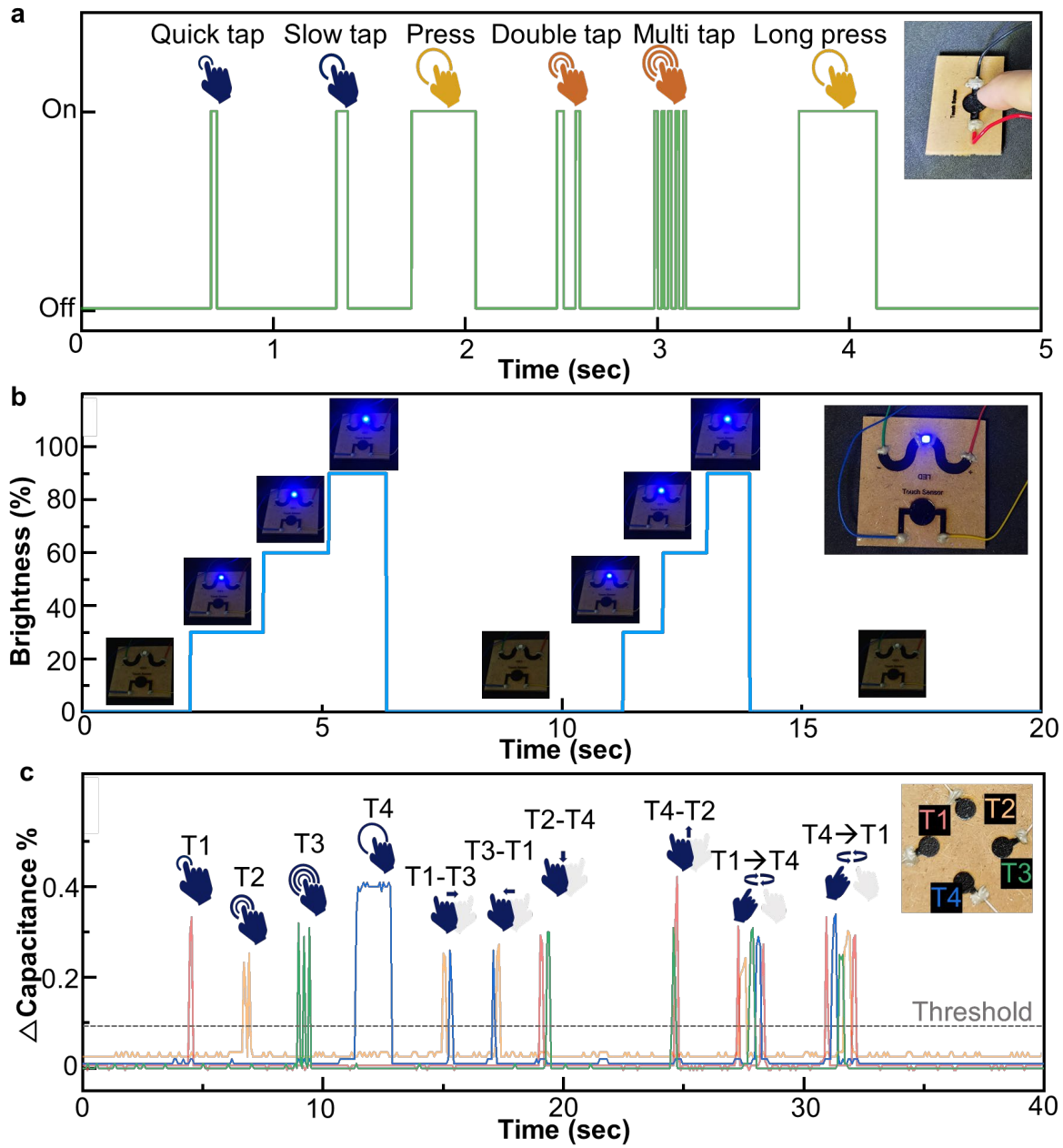

Figure 3. LIG touch sensors Fabrication. **(a)** Touch sensor on-off control. **(b)** Touch sensor LED brightness control. **(c)** Multi touch sensors control.

[Joule heating-based LIG Heater on MDF and Its Touch-Sensor-based Control]

The FsLDW LIG electrodes on MDF served as a Joule heating-based heater, as depicted in Figure 4. This setup leverages the inherent resistance of LIG to the conversion of electrical energy into thermal energy via the Joule heating method, achieved by connecting it to a power source to apply electricity. Considering that MDF's ignition point lies within the range of 200 ℃ to 275 ℃, the testing was conducted under these pertinent conditions. According to the literature, the thermal conductivity of LIG is notably high compared to wood, measuring at 1.72 W/m·K.[68] Given that thermal conductivity typically correlates with electrical conductivity, it's

anticipated that our LIG, which exhibits superior electrical conductivity compared to previously reported LIG, would also demonstrate even higher thermal conductivity. Conversely, the thermal conductivity of MDF is relatively low, exceeding 0.12 W/m·K.[69] In our experiments, conducted up to 170 ℃ or lower, we observed no indications of substrate carbonization in the MDF. In contrast, common cookware is typically metallic, boasting high heat conductivity. This implies that most heat generated by the LIG heater will efficiently transfer to the cookware, minimizing heat dissipation to the surroundings. Because temperatures below 200 ℃, which suffice for most cooking purposes, remain below the ignition point of MDF, along with thermal conductivity characteristics, the possibility of fire risk is low. Figure 4a illustrates the stepwise elevation of set voltage levels during heater testing, resulting in gradual temperature stabilization owing to the consistent supply voltage to the LIG heater. At a voltage of 5 V and a current of 0.4 A, a temperature of 161.5 ℃ was attained, sustaining stable levels without fluctuation. Figure 4b showcases temperature ascent and stabilization in tandem with incremental power increase during stepwise voltage elevation, with the power supply intermittently halted at the stabilization stage to cool to room temperature before subsequent voltage application. During this experiment, it was verified that the maximum temperature of 148.64 °C was consistently attained under the specified conditions of 1.2 W (8 V, 0.15 A). Moreover, the average time required to return from each target temperature to room temperature was found to be 236.4 seconds, attributable to the low thermal conductivity inherent to the MDF substrate. Nonetheless, the high thermal conductivity of LIG is evidenced by the rapid return of all heaters to room temperature within a mere 4-minute span, even when subjected to elevated temperatures. Moreover, this resilience of MDF to elevated temperatures, in contrast to solid wood, is attributed to its robust and dense structure achieved through the incorporation of thermal compression within the manufacturing process, along with the utilization of low-moisture content bonding agents inherent to MDF fabrication. This combination serves to effectively mitigate both volume changes and distortion tendencies, ensuring a relatively restrained response. Furthermore, replicating the stove warmer design, the LIG heater's heat distribution was evaluated, affirming uniform heat generation across most regions, as illustrated in Figure S6. Ultimately, Figure 4c exemplifies the integration of the LIG touch sensor with the LIG heater, demonstrating mutual control. The rectangular LIG served as a heater, while the dumbbell-designed LIG electrode, operating as a touch sensor via PWM modulation, regulated the electric power voltage. The power supply can provide an output voltage of up to 12 V, and the LIG heater can maintain consistent temperatures suitable for food heating. By gradually increasing the supply voltages to 1.2, 2.4, and 3.6 V using the LIG touch sensor, the LIG heater

reached temperatures of 40, 70, and 103 °C, respectively, further substantiating its potential as an effective heating element for culinary applications.

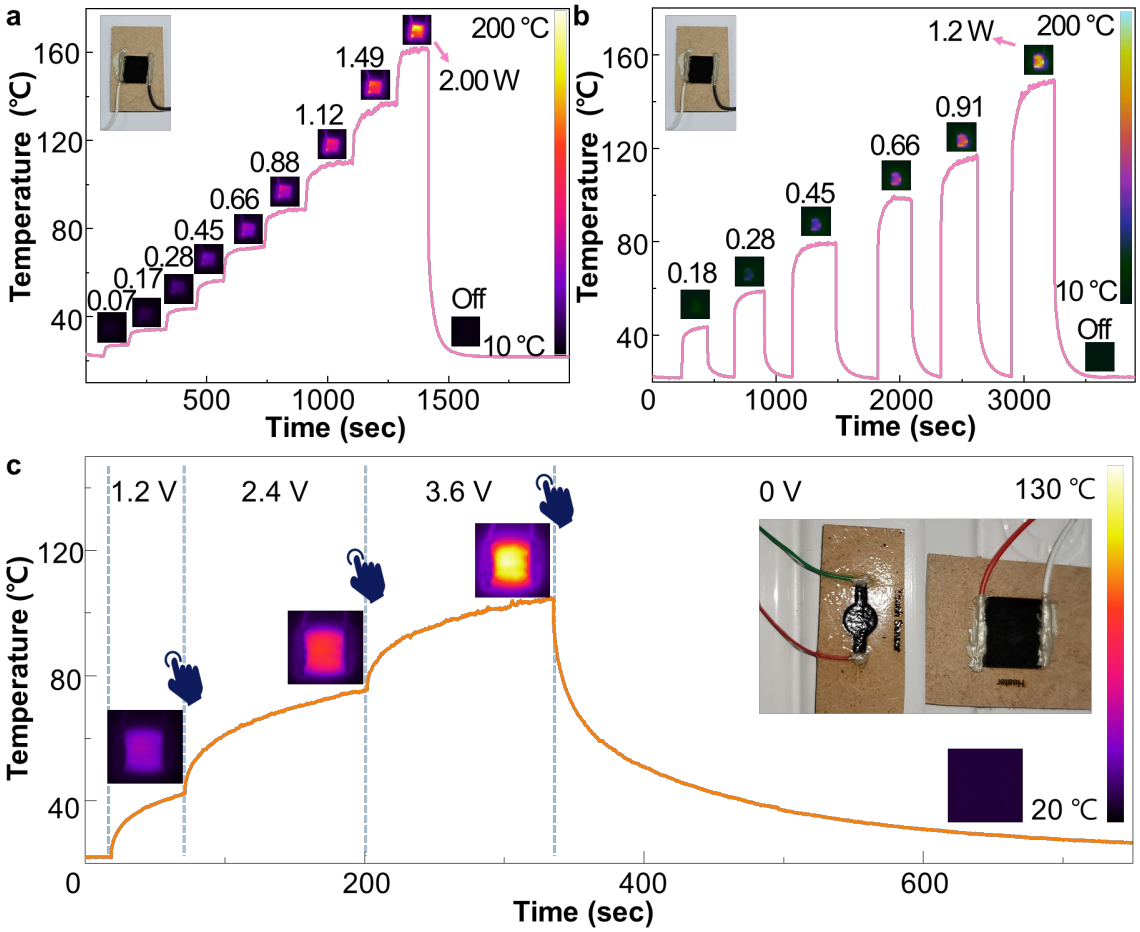

Figure 4. Characterization of the LIG heater on MDF. **(a)** Temperature profile of an LIG heater on MDF with incremental increases in applied DC bias and the corresponding IR images. **(b)** Temperature profile of an LIG heater with different voltages for monitoring the stabilization time in each condition. **(c)** Temperature control of LIG heater by LIG touch sensor and the corresponding IR images.

3. Conclusion

In this research, the utilization of FsLDW technology for LIG fabrication was extended to recycled wooden substrates, encompassing MDF, PCB, LCP, and OSB. Through optimization, high-quality LIG electrodes were fabricated into MDF, serving as electrodes for supplying electricity for lighting, touch sensors, and heaters to realize environmentally conscious smart furniture. Notably, these feats were accomplished within the ambient air, leveraging femtosecond lasers with near-infrared wavelength and ultrashort pulse duration, while minimizing thermal damage and eschewing intricate fabrication processes. This approach

culminated in the production of high-quality LIG electrodes on MDF, boasting the highest electrical conductivity of 2.781 Ω sq^{-1}, surpassing past lignocellulosic materials-based LIG electrodes. A capacitive LIG touch sensor was seamlessly woven into the MDF, with its efficacy as a smart sensor assessed through multifaceted tests, encompassing on-off control, PWM modulation of light intensity control, and multi-touch sensing. Leveraging the simultaneous coordination of multiple touch sensors facilitated effective computer control. Additionally, a Joule heating-based LIG heater was harnessed, demonstrating steady operation up to 160 ℃ without fluctuations. Heater Control via the touch sensor showcased its applicability for functions such as coffee boiling or stove warming, directly on a tangible surface. These comprehensive experiments collectively underscore the capacity of FsLDW technology-fabricated LIG on MDF to cater to both mass production and personalized manufacturing, aligning with individualized requirements. Furthermore, harnessing wooden materials to fabricate biodegradable and biocompatible carbon electrodes at high speed and low cost through fs laser irradiation, without additional chemicals, impeccably aligns with the requirements of green electronics. This technology holds promise in imparting smart functionalities to a diverse range of recycled wood-based furniture, fostering the creation of affordable, high-quality, eco-conscious furniture with ease, rapidity, and cost-effectiveness. Embedded within this outcome lies the resolution to the persistent recycling challenge faced by smart furniture, highlighting its capacity to seamlessly integrate sustainability and convenience.

4. Experimental Section

One-step Fabrication of FsLDW-based LIG on Recycled Wood: Patterning Details

Recycled woods including MDF, PB, OSB, and LCP, were prepared and cut into desired size for experimentation. The application of FsLDW technology at ambient room temperature, without the need for any specific pre-treatment, facilitated the fabrication of high-quality LIG electrodes under various laser power and scan speed parameters. Our FsLDW setup, illustrated in Figure S7, incorporates diverse optical components for precise beam delivery to the samples from fs laser, along with Galvano scanners and an f-theta lens. Utilizing a 255-fs pulse duration, 1040 nm near-IR wavelength, 201.5 kHz repetition rates, and a maximum 7 W ytterbium-doped fiber femtosecond laser (Lasernics, FUPL-250-6), we directly produced one-step LIG electrodes in ambient air, without supplementary chemical processes. The laser pulses, guided by a series of optical elements including half wave plates and a polarized beam splitter, were precisely controlled for polarization and power through careful adjustments. The initial half-wave plate (HWP) serves to convert the randomly polarized laser beam emitted by the laser

into linearly polarized light. Subsequently, at the polarized beam splitter (PBS), the beam from the HWP undergoes separation into P waves and S waves, with the p-polarized light being transmitted and the S-polarized light wave being reflected and absorbed into the beam block (BB). This characteristic enables precise adjustment of the laser power by manipulating the angle of the first HWP. Following this, the second HWP further adjusts the polarization to reach the sample. Although we aimed to investigate potential differences in LIG performance based on polarization effects, we found that the polarization effect was negligible due to the LIG generation mechanism being primarily governed by photothermal accumulation. After this stage, the laser beam proceeds through two mirrors before reaching the galvano scanner. The laser was then scanned utilizing a Galvano scanner (PSXA 104A), which features two computer-programmable Galvano mirrors, as per our specified design. Achieving high-resolution patterning necessitated the focal capabilities of an F-theta lens (Wavelength Optoelectronics, SL-1064-50-100), yielding a focused beam size of 77×71 μm, characterized by an oval shape. To optimize results, laser power (ranging from 0.8 W to 3.0 W) and scan speed (modulated between 10 mm/s and 90 mm/s) were systematically adjusted. All experimental procedures were conducted within ambient air conditions (20-25 °C, 35-55% relative humidity), and no drying or additional chemical treatments were applied throughout the process. As indicated in Tables S1-S4, the fabricated LIG electrodes underwent measurements using a Source Measurement Unit (SMU; Keysight, B2912A) and a 4-Point Probe (MS Tech, M4P-302). The outcomes confirmed the achievement of a high quality LIG electrode, optimized under the conditions of 2W laser power and a scanning speed of 30 mm/s, securely formed to the MDF substrate. The fabricated LIG electrode stands out with the lowest sheet resistance value when compared to previously introduced LIG electrodes based on lignocellulosic materials in various prior studies. Comprehensive information regarding the experimental conditions, performance outcomes, and laser parameters from these earlier investigations and this study is compiled in Table 1 and Table S5.

Material Characterization

At a laser power of 2 W with different scanning speeds, LIG electrodes were manufactured on MDF, and their surface profile and porous structure were examined through SEM (FEI Company, Magellan 400) analysis. Moreover, the ablation depth and average roughness of both the MDF and the LIG electrode were assessed utilizing a Confocal Microscope (Keyence, VK-X200). The analysis extended to Raman spectroscopy, performed at room temperature employing a HORIBA LabRAM ARAMIS dispersive spectrometer equipped with a 50 X

objective lens. The Raman spectrum analysis used a 633 nm wavelength laser light source and 1200 lines per mm grating, and data were accumulated five times, each for a duration of 10 seconds, to capture G, D, and 2D Raman peaks. Additionally, XPS data were gathered utilizing a Thermofisher Nexa G2 apparatus at pressures of 10^{-8} Torr, employing Al-Kα radiation (1486.7 eV) to elucidate surface chemical elements. Both LIG and MDF samples were processed into powder form and subjected to a variety of analyses, encompassing TGA, XRD, and FTIR (Fourier-transformed) spectroscopy. Thermal stability analysis encompassed temperature increments from room temperature to 1000 °C, with a heating rate of 10 °C min^{-1}, performed using a TGA (NETZSCH TG209F1 Libra) instrument. XRD characterization of LIG utilized a RIGAKU SmartLab instrument with Cu-Kα radiation (1.541 Å) source, X-ray generator (maximum 9 kW), goniometer (300 mm radius), secondary monochromator, and hybrid detector in 0/1/2D mode. The prepared LIG and MDF powders were mixed with KBr powder, compacted into thin disks under pressure, and subjected to FTIR spectroscopy (Thermo Scientific, Nicolet iS50), as illustrated in Figure S8. A pronounced broad dip within the 3000 to 3700 cm^{-1} range on the MDF spectrum corresponds to an O–H signal, linked to moisture content in the material. However, the carbonization and graphitization processes induced by femtosecond laser treatment have led to a reduction in the O-H dip intensity in the LIG spectrum. The stretching vibrations responsible for C–O, C–O–C, and C=C features in the wood material also largely diminish during the MDF to LIG conversion. This outcome suggests that the femtosecond laser pulses have effectively removed most of the oxygen-containing functional groups present in MDF, and a portion of the carbon constituents have transformed into a stable aromatic carbon ring network.

LIG Electrodes for Green Smart Furniture

Manufactured under ideal conditions (2 W laser power, 30 mm/s scanning speed), the LIG-based electrodes performed diverse functions, providing electricity for lighting, enabling touch sensing, and facilitating heating applications. To enhance durability, a wood varnish coating was applied to the fabricated LIG sensors and electrodes, drawing on a known protective strategy.[70] These LIG touch sensors were linked to a CBB (Capacitive breakout board; Adafruit, MPR121), which communicated with a microcontroller (Atmel, ATmega32u4). Upon pressing each LIG sensor, digital sensing data from the CBB was transmitted to the microcontroller for processing, subsequently modulating external devices (LED, Heater, PC) through PWM output pins based on CBB signals. Specifically, the variation in capacitance between touch and release instances was gathered and underwent processing via a filtration system introduced in previous

study.[70] The touch sensor shown in Figure 3a demonstrates real-time response monitoring upon contact and release. It achieves this by transmitting a value of 1 when pressed and 0 when released, enabling comprehensive on-off control. Similarly, Figure 3b illustrates the linkage of an LED to the microcontroller's PWM output, enabling adjustable brightness. Upon touch, guided by the CBB signal, the microcontroller modulates PWM from 0 to 255. Table S6 presents data showcasing PWM's codes on light brightness corresponding to the number of touches. In this specific experiment, LED intensity is regulated at 30% for the first touch, 60% for the second, 90% for the third, and switched off after the last touch. The regulation of lighting intensity can be adjusted as per the specific application by modifying input codes. To facilitate PC control using the LIG touch sensor (depicted in Figure 3c, Figure S5, and Video S1), the microcontroller was connected to the PC. Each touch sensor unit was designated as a keyboard pin-out, with individual shortcut keys assigned to different sensors. This setup allowed for the recognition of single-touch and continuous-touch operations as a single shortcut key, as demonstrated in Table S7. The feasibility of computer control through the placement of pins on each LIG touch sensor unit, assigning specific functions for touch and multi-touch control, was corroborated. The LIG heaters illustrated in Figure 4a and 4b, were linked to a power supply (Keysight, U8032A) to regulate temperature. The real-time temperature measurement at varying voltages was carried out using IR cameras (FLIR, A35). In the final depiction, Figure 4c and Video S2 reveal the orchestrated control of the LIG heater by the LIG touch sensor. This was achieved by connecting the LIG heater to the DC motor control chip (L9110, ASIC), with voltage regulation facilitated by the microcontroller as seen in Figure S9. The microcontroller enabled temperature control by supplying voltages (ranging from 0 to 12 V) in accordance with the CBB signal's PWM method upon touch sensor activation. This experiment employed voltages of 1.2 V, 2.4 V, 3.6 V, and 0 V, determined by the number of touches required to attain target temperatures.

Author Contributions

H.K.N. and Y.-J.K. conceived the idea and designed the experiments and prepared the manuscript. H.K.N., J.C., and T.J. carried out heater and sensor experiments. H.K.N., D.Y., Y.L., and Y.-R.K. performed sample fabrication. H.K.N., T.-S.D.L., and B.K. conducted characterizations. H.K.N., L. Yu, S.-W.K., I.P., and Y.-J.K. supervised over all the experiments. All authors contributed significant discussions for final paper polishing.

Declaration of Competing Interest

The authors declare that they have no known competing financial interests or personal relationships that could have appeared to influence the work reported in this paper.

Supporting Information

Supporting Information is available from the Wiley Online Library or from the author.

Acknowledgements

This work was supported by the National Research Foundation of the Republic of Korea (NRF-2021R1A4A103166012), the R&D Program for Forest Science Technology (Project No. 2023488B10-2325-AA01) provided by Korea Forest Service (Korea Forestry Promotion Institute), and the Basic Research Program (NK242C-02) funded by the Korea Institute of Machinery and Materials (KIMM). This work was also supported by Korea Institute of Planning and Evaluation for Technology in Food, Agriculture and Forestry (IPET) funded by Ministry of Agriculture, Food and Rural Affairs (MAFRA) (321077-2).

Received: ((will be filled in by the editorial staff))

Revised: ((will be filled in by the editorial staff))

Published online: ((will be filled in by the editorial staff))

References

1. Wang F, Harindintwali JD, Yuan Z, et al. Technologies and perspectives for achieving carbon neutrality. *Innovation*. 2021;2(4).
2. Chen JM. Carbon neutrality: Toward a sustainable future. *Innovation*. 2021;2(3).
3. ARRow KJ, Cohen L, DAviD PaA, et al. *A Statement on the Appropriate Role for Research and Development in Climate Policy*.
4. Lamb WF, Wiedmann T, Pongratz J, et al. A review of trends and drivers of greenhouse gas emissions by sector from 1990 to 2018. *Environmental Research Letters*. 2021;16(7).
5. Mehta S, Jha S, Liang H. Lignocellulose materials for supercapacitor and battery electrodes: A review. *Renewable and Sustainable Energy Reviews*. 2020;134.
6. Heräjärvi H, Kunttu J, Hurmekoski E, Hujala T. Outlook for modified wood use and regulations in circular economy. *Holzforschung*. 2020;74(4):334-343.
7. Chen C, Kuang Y, Zhu S, et al. Structure–property–function relationships of natural and engineered wood. *Nat Rev Mater*. 2020;5(9):642-666.
8. Ge S, Shi Y, Chen X, et al. Sustainable upcycling of plastic waste and wood fibers into high-performance laminated wood-polymer composite via one-step cell collapse and chemical bonding approach. *Adv Compos Hybrid Mater*. 2023;6(4):146.
9. Song J, Chen C, Zhu S, et al. Processing bulk natural wood into a high-performance structural material. *Nature*. 2018;554(7691):224-228.

10. Ye H, Shi Y, Xu B Bin, et al. Sustainable ultra-strong thermally conductive wood-based antibacterial structural materials with anti-corrosion and ultraviolet shielding. *EcoMat*. 2023;5(12).
11. Xiao S, Chen C, Xia Q, et al. Lightweight, strong, moldable wood via cell wall engineering as a sustainable structural material. *Science (1979)*. 2021;374(6566):465-471.
12. Zhu M, Song J, Li T, et al. Highly Anisotropic, Highly Transparent Wood Composites. *Advanced Materials*. 2016;28(26):5181-5187.
13. Ge S, Ouyang H, Ye H, Shi Y, Sheng Y, Peng W. High-performance and environmentally friendly acrylonitrile butadiene styrene/wood composite for versatile applications in furniture and construction. *Adv Compos Hybrid Mater*. 2023;6(1):44.
14. Ding Y, Pang Z, Lan K, et al. Emerging Engineered Wood for Building Applications. *Chem Rev*. 2023;123(5):1843-1888.
15. Mi R, Li T, Dalgo D, et al. A Clear, Strong, and Thermally Insulated Transparent Wood for Energy Efficient Windows. *Adv Funct Mater*. 2020;30(1).
16. Li T, Zhai Y, He S, et al. A radiative cooling structural material. *Science (1979)*. 2019;364(6442):760-763.
17. Geng A, Ning Z, Zhang H, Yang H. Quantifying the climate change mitigation potential of China's furniture sector: Wood substitution benefits on emission reduction. *Ecol Indic*. 2019;103:363-372.
18. Epede MB, Wang D. Competitiveness and upgrading in global value chains: A multiple-country analysis of the wooden furniture industry. *For Policy Econ*. 2022;140.
19. Blažević D, Bukovčan M, Keser T, Nenadić K. Conceptual Design of Smart Furniture: A Case Study. *30th International Conference on Organization and Technology of Maintenance (OTO 2021)*. 2022;369:353-363.
20. Krejcar O, Maresova P, Selamat A, et al. Smart Furniture as a Component of a Smart City—Definition Based on Key Technologies Specification. *IEEE Access*. 2019;7:94822-94839.
21. Wan J, Song J, Yang Z, et al. Highly Anisotropic Conductors. *Advanced Materials*. 2017;29(41).
22. Guo H, Büchel M, Li X, Wäckerlin A, Chen Q, Burgert I. Dictating anisotropic electric conductivity of a transparent copper nanowire coating by the surface structure of wood. *J R Soc Interface*. 2018;15(142):20170864.
23. Du B, Jiang J, Li J, Zhu W. Effects of ZnO magnetron sputtering on surface charge and flashover voltage of oil-impregnated paper. *High Voltage*. 2019;4(4):308-315.
24. Lin F, Qiu Y, Zheng X, et al. One-pot mechanochemical assembly of lignocellulose nanofiber/graphite nanocomposites for wearable electronic devices. *Chemical Engineering Journal*. 2022;437:135286.
25. Li W, Liu Q, Zhang Y, et al. Biodegradable Materials and Green Processing for Green Electronics. *Advanced Materials*. 2020;32(33).
26. Irimia-Vladu M. "Green" electronics: biodegradable and biocompatible materials and devices for sustainable future. *Chem Soc Rev*. 2014;43(2):588-610.
27. Ye R, Chyan Y, Zhang J, et al. Laser-Induced Graphene Formation on Wood. *Advanced Materials*. 2017;29(37).
28. Ye R, James DK, Tour JM. Laser-Induced Graphene: From Discovery to Translation. *Advanced Materials*. 2019;31(1).
29. Chyan Y, Ye R, Li Y, Singh SP, Arnusch CJ, Tour JM. Laser-Induced Graphene by Multiple Lasing: Toward Electronics on Cloth, Paper, and Food. *ACS Nano*. 2018;12(3):2176-2183.

30. Trusovas R, Ratautas K, Račiukaitis G, Niaura G. Graphene layer formation in pinewood by nanosecond and picosecond laser irradiation. *Appl Surf Sci*. 2019;471:154-161.
31. Le TSD, Lee YA, Nam HK, et al. Green Flexible Graphene–Inorganic-Hybrid Micro-Supercapacitors Made of Fallen Leaves Enabled by Ultrafast Laser Pulses. *Adv Funct Mater*. 2022;32(20).
32. Nam HK, Le TSD, Yang D, et al. Smart Wooden Home Enabled by Direct-Written Laser-Induced Graphene. *Adv Mater Technol*. Published online 2023.
33. Pinheiro T, Silvestre S, Coelho J, et al. Laser-Induced Graphene on Paper toward Efficient Fabrication of Flexible, Planar Electrodes for Electrochemical Sensing. *Adv Mater Interfaces*. 2021;8(22).
34. Jung Y, Min JK, Choi J, et al. Smart paper electronics by laser-induced graphene for biodegradable real-time food spoilage monitoring. *Appl Mater Today*. 2022;29.
35. Imbrogno A, Islam J, Santillo C, et al. Laser-Induced Graphene Supercapacitors by Direct Laser Writing of Cork Natural Substrates. *ACS Appl Electron Mater*. 2022;4(4):1541-1551.
36. Gomez-Martin A, Martinez-Fernandez J, Ruttert M, Winter M, Placke T, Ramirez-Rico J. Porous Graphene-like Carbon from Fast Catalytic Decomposition of Biomass for Energy Storage Applications. *ACS Omega*. 2019;4(25):21446-21458.
37. Popov V V., Orlova TS, Magarino EE, Bautista MA, Martínez-Fernández J. Specific features of electrical properties of porous biocarbons prepared from beech wood and wood artificial fiberboards. *Physics of the Solid State*. 2011;53(2):276-283.
38. Dodevski V, Janković B, Stojmenović M, et al. Plane tree seed biomass used for preparation of activated carbons (AC) derived from pyrolysis. Modeling the activation process. *Colloids Surf A Physicochem Eng Asp*. 2017;522:83-96.
39. Tang MM, Bacon R. Carbonization of cellulose fibers—I. Low temperature pyrolysis. *Carbon N Y*. 1964;2(3):211-220.
40. Bacon R, Tang MM. Carbonization of cellulose fibers—II. Physical property study. *Carbon N Y*. 1964;2(3):221-225.
41. de Paiva MV, Bettini J, Colombari FM, Fazzio A, Strauss M. Unveiling electrical anisotropy of hierarchical pyrolytic biocarbons from wood cellulose. *J Mater Sci*. 2022;57(48):21980-21995.
42. Lower L, Dey SC, Vook T, Nimlos M, Park S, Sagues WJ. Catalytic Graphitization of Biocarbon for Lithium-Ion Anodes: A Minireview. *ChemSusChem*. 2023;16(24).
43. Chen C, Chen Y, Zhu S, et al. Catalyst-Free *In Situ* Carbon Nanotube Growth in Confined Space *via* High Temperature Gradient. *Research*. 2018;2018.
44. Kim B, Nam HK, Watanabe S, et al. Selective Laser Ablation of Metal Thin Films Using Ultrashort Pulses. *International Journal of Precision Engineering and Manufacturing - Green Technology*. 2021;8(3):771-782.
45. Le TSD, Park S, An J, Lee PS, Kim YJ. Ultrafast Laser Pulses Enable One-Step Graphene Patterning on Woods and Leaves for Green Electronics. *Adv Funct Mater*. 2019;29(33).
46. Haller P, Beyer E, Wiedemann G, Panzner M, Wust H. Experimental study of the effect of a laser beam on the morphology of wood surfaces. *Wood composites and chemistry : International symposium*. 2002;(January 2002):83-91.
47. Roth P, Filippov AV. In situ ultrafine particle sizing by a combination of pulsed laser heatup and particle thermal emission. *J Aerosol Sci*. 1996;27(1):95-104.
48. Han X, Ye R, Chyan Y, et al. Laser-Induced Graphene from Wood Impregnated with Metal Salts and Use in Electrocatalysis. *ACS Appl Nano Mater*. 2018;1(9):5053-5061.
49. Dreimol CH, Guo H, Ritter M, et al. Sustainable wood electronics by iron-catalyzed laser-induced graphitization for large-scale applications. *Nat Commun*. 2022;13(1).

50. Miyakoshi R, Hayashi S, Terakawa M. Simultaneous laser-based graphitization and microstructuring of bamboo for supercapacitors derived from renewable resources. *RSC Adv*. 2022;12(46):29647-29652.
51. Kulyk B, Silva BFR, Carvalho AF, et al. Laser-Induced Graphene from Paper for Mechanical Sensing. *ACS Appl Mater Interfaces*. 2021;13(8):10210-10221.
52. Chyan Y, Cohen J, Wang W, Zhang C, Tour JM. Graphene Art. *ACS Appl Nano Mater*. 2019;2(5):3007-3011.
53. Stanford MG, Li JT, Chyan Y, Wang Z, Wang W, Tour JM. Laser-Induced Graphene Triboelectric Nanogenerators. *ACS Nano*. 2019;13(6):7166-7174.
54. Carvalho AF, Fernandes AJS, Martins R, Fortunato E, Costa FM. Laser-Induced Graphene Piezoresistive Sensors Synthesized Directly on Cork Insoles for Gait Analysis. *Adv Mater Technol*. 2020;5(12).
55. Silvestre SL, Pinheiro T, Marques AC, et al. Cork derived laser-induced graphene for sustainable green electronics. *Flexible and Printed Electronics*. 2022;7(3).
56. Lin Y, Zhang Q, Deng Y, et al. Fabricating Graphene and Nanodiamonds from Lignin by Femtosecond Laser Irradiation. *ACS Omega*. 2021;6(49):33995-34002.
57. Mahmood F, Mahmood F, Zhang H, Lin J, Wan C. Laser-Induced Graphene Derived from Kraft Lignin for Flexible Supercapacitors. *ACS Omega*. 2020;5(24):14611-14618.
58. Funayama R, Hayashi S, Terakawa M. Laser-Induced Graphitization of Lignin/PLLA Composite Sheets for Biodegradable Triboelectric Nanogenerators. *ACS Sustain Chem Eng*. 2023;11(7):3114-3122.
59. Pereira CR, Mölleken RE, de Souza FH, Capellari GS, Neto SC, Azevedo EC. Evaluation of MDF bonding with polyurethane of castor oil. *Applied Adhesion Science*. 2016;4(1).
60. Gutiérrez-Pardo A, Ramírez-Rico J, de Arellano-López AR, Martínez-Fernández J. Characterization of porous graphitic monoliths from pyrolyzed wood. *J Mater Sci*. 2014;49(22):7688-7696.
61. Chen Y, Long J, Zhou S, et al. UV Laser-Induced Polyimide-to-Graphene Conversion: Modeling, Fabrication, and Application. *Small Methods*. 2019;3(10).
62. Miyamoto Y, Zhang H, Tománek D. Photoexfoliation of graphene from graphite: An Ab initio study. *Phys Rev Lett*. 2010;104(20).
63. Sokolowski-Tinten K, Solis J, Bialkowski J, Siegel J, Afonso CN, von der Linde D. Dynamics of Ultrafast Phase Changes in Amorphous GeSb Films. *Phys Rev Lett*. 1998;81(17):3679-3682.
64. Gaudin J, Peyrusse O, Chalupský J, et al. Amorphous to crystalline phase transition in carbon induced by intense femtosecond x-ray free-electron laser pulses. *Phys Rev B*. 2012;86(2):024103.
65. Loh GC, Baillargeat D. Graphitization of amorphous carbon and its transformation pathways. *J Appl Phys*. 2013;114(3).
66. Vashisth A, Kowalik M, Gerringer JC, Ashraf C, Van Duin ACT, Green MJ. ReaxFF Simulations of Laser-Induced Graphene (LIG) Formation for Multifunctional Polymer Nanocomposites. *ACS Appl Nano Mater*. 2020;3(2):1881-1890.
67. Dong Y, Rismiller SC, Lin J. Molecular dynamic simulation of layered graphene clusters formation from polyimides under extreme conditions. *Carbon*. 2016;104:47-55.
68. Wang Z, Wang G, Liu W, Hu B, Liu J, Zhang Y. Patterned laser-induced graphene for terahertz wave modulation. *Journal of the Optical Society of America B*. 2020;37(2):546.
69. Sonderegger W, Niemz P. Thermal conductivity and water vapour transmission properties of wood-based materials. *European Journal of Wood and Wood Products*. 2009;67(3):313-321.

70. Oh S, Lee S, Byun SH, et al. 3D Shape-Morphing Display Enabled by Electrothermally Responsive, Stiffness-Tunable Liquid Metal Platform with Stretchable Electroluminescent Device. *Adv Funct Mater*. 2023;33(24).

The table of contents entry should be 50–60 words long and should be written in the present tense. The text should be different from the abstract text.

Laser-Induced Graphene Formation on Recycled Woods for Green Smart Furniture

Han Ku Nam, Jungrak Choi, Tongmei Jing, Dongwook Yang, Younggeun Lee, Young-Ryeul Kim, Truong-Son Dinh Le, Byunggi Kim, Liandong Yu, Seung-Woo Kim, Inkyu Park, and Young-Jin Kim*

We demonstrate the direct patterning of femtosecond Laser-Induced Graphene (LIG) onto recycled wood, creating key electrical components for green smart furniture. These LIG electrodes set a record-breaking electrical conductivity record at 2.781 Ω sq^{-1} among lignocellulosic LIGs. Our LIG-based capacitive touch sensor controls the light brightness, adjusts the stove warmer temperature, and operates the computer interface.

ToC figure (Please choose one size: 55 mm broad × 50 mm high **or** 110 mm broad × 20 mm high. Please do not use any other dimensions)